Available online at www.sciencedirect.com
SCIENCE DIRECT®
European Journal of Mechanics B/Fluids 24 (2005) 555–571

The dynamics of a moving sheet of liquid, part I: derivation of the 2D equations of motion

M. Gilio, F. Al-Bender *, J.-P. Kruth

Katholieke Universiteit Leuven, Department of Mechanical Engineering, Celestijnenlaan 300B, 3001 Heverlee, Belgium

Received 28 January 2003; received in revised form 9 September 2004; accepted 13 December 2004

Available online 12 February 2005

Abstract

In order to investigate the transient response of a planar liquid sheet, subjected to deflection due to inertia forces, a mathematical description of the time-dependent behaviour of a liquid sheet is needed. This paper discusses the derivation of the equations of motion governing the time-dependent deflection of a moving sheet of liquid. The magnitude of the deflection considered is on the order of magnitude of the sheet's length, and the Reynolds number considered is small. The equations are expressed within a 2D orthogonal curvilinear co-ordinate system, moving and changing shape along with the sheet. The co-ordinate system's motion is described by a specific velocity component, and is imposed by the motion of the slot from which the sheet emanates. The derived equations include viscous contributions to the sheet's dynamics and are general enough to allow comparison with special cases found in previous literature works. The influence of viscosity on the sheet's dynamics is assessed by numerical computations of the derived equations.

Keywords: Liquid sheet; Curtain coating; Curvilinear co-ordinate; Time-dependent

1. Introduction

Planar liquid sheets are encountered in various industrial coating processes. Coating processes that use a liquid sheet are generally referred to as *curtain coating* processes. Coating happens by impingement of the liquid sheet onto a moving substrate, such as photographic or magnetic carrier films. In these cases the liquid sheet is extruded from a fixed mounted die, while the substrate is moving underneath the sheet. A comprehensive overview of coating methods may be found in Kistler and Schweizer [1].

On the other hand, one may think of an application where a planar liquid sheet moves, while the substrate that is to be coated stands still. An example of the latter is *curtain recoating for stereolithography* [2,3]. Stereolithography (SL) is a manufacturing process, where parts are grown in a layerwise fashion by selectively curing a liquid photopolymer with a laser beam. The process consists of a repetition of two distinct phases. In a first phase, a liquid film is coated onto a bath of liquid, in which the

* Corresponding author.
E-mail address: farid.al-bender@mech.kuleuven.ac.be (F. Al-Bender).

0997-7546/$ – see front matter
doi:10.1016/j.euromechflu.2004.12.003

Nomenclature

a_D	acceleration of the coating die	u	streamwise velocity
f	normal velocity of the sheet's centre line	u_s	streamwise velocity scale ($\sqrt{gL}$)
g	gravitational acceleration	v	velocity component normal to sheet's centre line
H	slot clearance		
h	element of length ($1+n\kappa$)	W	modified Weber number ($\rho u_s^2 L\sigma^{-1}$)
L	sheet length	We	Weber number ($\rho u_s^2 T_0\sigma^{-1}$)
p	liquid pressure	ε	slenderness ratio ($T_0 L^{-1}$)
p^g	gas pressure	θ	angle of the sheet's centre line with the vertical axis
Q	flow rate per unit sheet width		
R	modified Reynolds number ($\rho u_s L\mu^{-1}$)	κ	curvature of the sheet's centre line ($\partial\theta/\partial s$)
Re	Reynolds number ($\rho u_s T_0\mu^{-1}$)	κ_{if}	curvature of the air–liquid interface
T	sheet thickness	μ	dynamic viscosity
T_0	initial sheet thickness (at die outlet)	ρ	liquid density
t	time	σ	surface tension

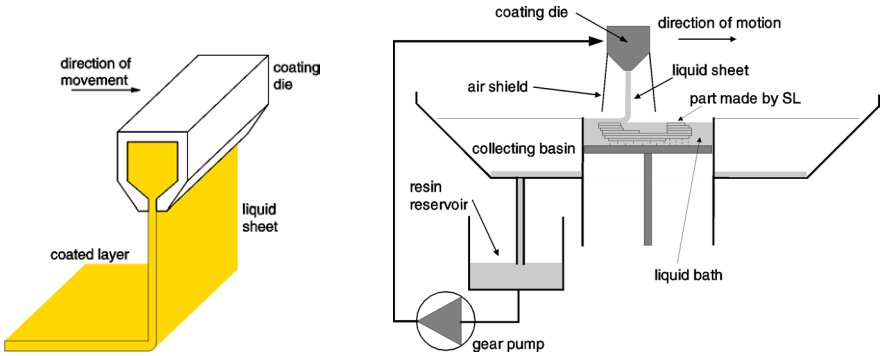

Fig. 1. Curtain recoating for stereolithography: coating of a new liquid layer. (a) Coating die extruding a liquid sheet, and coating of a liquid layer. (b) Schematic view of the machine and its layer coating process.

part is grown. The second phase consists of selectively curing a part's cross-section in the applied liquid film by scanning the surface with a laser beam.

Fig. 1 shows schematically the principle behind curtain recoating for stereolithography. A die extrudes a liquid sheet through a narrow slot at its lower face (Fig. 1(a)). Motion of the die and the liquid curtain causes a thin film of liquid to be coated. The curtain must move at a constant speed in order to coat a film of uniform thickness. The thickness d of the coated layers depends on the flow rate Q (expressed per unit sheet width) through the die, and on the coating speed V_C by the relation $d = Q \cdot V_C^{-1}$. Only the film coated onto the liquid bath (Fig. 1(b)), in which the part to be made is grown, is useful. During acceleration and deceleration of die and curtain, the impinging liquid is collected in a basin and flows back to a reservoir. After a new liquid layer has been coated, it is selectively cured by an UV-laser beam. In this way, the part grows by one layer. The whole process is repeated several times, until all layers that constitute the part have been added.

The motion of the coating die is repetitive, meaning that the die is moved from one end of the machine to the other and vice versa, each time coating a single layer. The motion of the die consists of an acceleration phase, a phase of constant speed – during which the layer is coated onto the bath of liquid, and a deceleration phase. When the die is accelerated, the liquid sheet experiences an inertia force, that tends to bend the liquid sheet out of its plane, giving rise to a transient response. This transient response must have dissipated when coating of a layer starts, otherwise leading to an irregularly coated layer. The faster the transient response decays, the shorter the machine stroke can be for a given coating speed, or the higher the coating speed can be for a given machine length.

In order to study the transient dynamics, a mathematical model of a liquid sheet is needed, able to predict the out-of-plane bending when the sheet undergoes a certain acceleration in function of time.

1.1. Literature overview

A large body of literature exists, addressing the mathematical description of the flow within a liquid sheet, and of its stability. However, the authors were not able to find works that derived equations of motion, describing the time-dependent deflection of a liquid sheet, when subjected to inertia forces. This paper considers sheet deflections that are on the order of magnitude of the sheet's length. A literature overview follows, discussing the works that are most relevant to the case being treated in this paper.

Extensive literature is available on the *steady-state* flow in 2D liquid sheets, and related stability. Brown [4] was perhaps the first to measure the streamwise velocity of steady, vertically falling viscous liquid sheets, for different viscosities and flow rates. Based on his experiments he proved that the streamwise velocity could be approximated by a modified free-fall velocity, in which the initial velocity was corrected for viscosity. Brown's formula is only a good approximation for distances sufficiently far downstream. In an appendix to the same paper, Taylor derived a differential equation for the streamwise velocity, assuming a constant normal stress, and neglecting surface tension. Choosing a co-ordinate system with x orientated towards streamwise direction, and y normal to it, and using $\bar{u}$ to denote the mean streamwise velocity, T the local sheet thickness, μ the dynamic viscosity, and g the gravitational acceleration, the equation derived by Taylor is expressed using the following dimensionless variables:

$$U = \left(\frac{\rho}{4\mu g}\right)^{1/3} \bar{u}, \qquad X = \left(\frac{\rho}{4\mu}\right)^{2/3} g^{1/3} x \tag{1}$$

and results in:

$$\frac{\mathrm{d}}{\mathrm{d}X}\left(\frac{1}{U}\frac{\mathrm{d}U}{\mathrm{d}X}\right) + \frac{1}{U} - \frac{\mathrm{d}U}{\mathrm{d}X} = 0. \tag{2}$$

The same equation (2) was later also derived by Clarke [5] as the leading order equation of a downstream asymptotic expansion for small Reynolds numbers.

Taylor's equation is valid downstream of a location in the sheet where the influence of the orifice on the flow has become sufficiently small. This influence is primarily due to viscous traction by the solid walls in the slot, which suddenly disappears at the orifice. The disappearing viscous traction causes a flow rearrangement in which the parabolic profile of streamwise velocity in the slot evolves to a plug-like profile. Gravity becomes increasingly important downstream to eventually dominate over viscous forces. Clarke hypothesised an exponentially fast decay of the orifice's influence on the flow in the curtain, giving as characteristic decay length the clearance of the slot, H. Söderberg and Alfredsson [6] provide proof for this assumption. They performed finite-difference calculations to investigate the relaxation of the streamwise and normal velocity profiles in case of a steady, 2D liquid sheet, issuing from a slot and falling in the direction of gravity. Assuming laminar flow in the slot, they found the relaxation length for the streamwise velocity u to be $\ell_R^u = 0.09HRe$. ℓ_R^u is calculated as the distance from the slot outlet where $|\frac{u_{\text{surface}}}{u_{\text{centreline}}} - 1| < 0.01$, and the Reynolds number is given by $Re = \rho Q \mu^{-1}$. For small Reynolds numbers, this means that the streamwise velocity u relaxes over a distance, which is less than the slot clearance. Thus, for long and thin (i.e. slender) sheets, the rearrangement zone close to the slot may be neglected.

Clarke [5] found an analytical solution of Taylor's equation (2) in terms of Airy functions:

$$U(X) = 2^{-1/3}\{Ai(r)\}^2 \big/ \left[\{Ai'(r)\}^2 - r \cdot \{Ai(r)\}^2\right]; \quad r = 2^{-1/3}(X + k_0) \tag{3}$$

where Ai is the Airy function, Ai' is its derivative with respect to r, and k_0 is an arbitrary constant. Adachi [7] proposed an approximate solution to Taylor's equation, overcoming the mathematical complexity of handling (3). His equation stems from an addition of two terms, governing respectively a viscous-gravity and inertia-gravity jet:

$$X = 1/2\left\{U^2 - \delta_i\left(\frac{\rho u_0^3}{4g\mu}\right)^{2/3}\right\} + 2^{1/2}\left\{U^{1/2} - \left(\frac{\rho u_0^3}{4g\mu}\right)^{1/6}\right\} \tag{4}$$

where δ_i is an integral constant, depending on the velocity profile ($\delta_i = 1$ for inviscid liquids), and u_0 is the mean streamwise velocity at slot outlet. The first term on the right-hand side is dominant in high-speed jets, and the second term in creeping jets. Eq. (4) may be used as a sufficient approximation of (3) if k_0 and δ_i are chosen appropriately.

Aidun [8] derived an equation governing the streamwise velocity in a planar sheet, starting from the Navier–Stokes (N–S) equations, integrating them over the sheet's thickness, and including appropriate boundary conditions at the free surface:

$$u\frac{\mathrm{d}u}{\mathrm{d}x} = \frac{4\mu}{\rho}\frac{\mathrm{d}^2u}{\mathrm{d}x^2} - \frac{1}{\rho T}\frac{\mathrm{d}T}{\mathrm{d}x}\left(\sigma\kappa + P_0 - 4\mu\frac{\mathrm{d}u}{\mathrm{d}x}\right) + g, \tag{5}$$

with σ the surface tension, and κ the curvature of the free surface. Taylor's equation results from (5) by neglecting surface tension, normalising pressure, such that the ambient pressure $P_0 = 0$, and converting to a dimensionless form using (1).

Further in his paper, Aidun used (5) to derive an approximate equation for the case of thin sheets, for which he neglects the curvature of the free surface such that $\mathrm{d}T/\mathrm{d}x$ is zero, leading to the equation

$$\frac{\mathrm{d}^2U}{\mathrm{d}X^2} = U\frac{\mathrm{d}U}{\mathrm{d}X} - 1,$$

with X and U expressed by (1). Using Brown's experimental data, he concluded Taylor's equation (2) to be the best one predicting the velocity measurements. Aidun's thin sheet approximation only agreed well with experimental data for $X > 3$, showing that $\mathrm{d}T/\mathrm{d}x$ is not negligible close to the slot exit. Brown's modified free-fall formula was only valid as an approximation for u for $X > 10$.

Ramos [9] used perturbation methods to derive leading-order equations of the N–S equations for planar liquid sheet flow at low Reynolds numbers. Neglecting surface tension, he showed Taylor's equation (2) to be the leading order approximation governing the streamwise velocity, for flow at low Reynolds numbers.

Concerning the deflection of liquid sheets, Buckmaster [10] analysed buckling phenomena of thin threads of viscous liquid falling nearly vertically through a bath of liquid of comparable density. Starting from the steady-state N–S equations, expressed in curvilinear orthogonal co-ordinates, he integrated them across the thread's thickness. To the resulting integral equations a perturbation analysis was applied to derive an equation describing the thread's path. The result was a fifth-order differential equation in the angle of the thread's centre line with the horizontal. The numerical solutions to this equation only partly accounted for the experimental observations. In a later paper, Buckmaster et al. [11] considered deformations of a thin 2D thread of viscous liquid, immersed in a vacuum, whose ends are moved slowly. They neglected therefore all inertia terms in their analysis, and made use of integrated equations to represent a global balance of forces and moments. Perturbation methods were used to derive an equation governing the thread's shape for the case where the deflection was of the order of (i) the thread's thickness, and (ii) the thread's length. Their procedure resulted, in both cases, in a third-order partial differential equation for the angle of the thread's centre line, as a function of time and distance from one end. For small deflections, the equations were linearised, and a complete discussion based on eigenfunction expansions was given. Solutions for large deflections necessitated numerical computations.

Another important matter of investigation is the dynamic response of liquid sheets to fluctuations in ambient pressure. Pressure fluctuations on the curtain due to air flow induce propagating waves that threaten uniform coating [12]. Ramos [13] studied the dynamic response of annular liquid jets to time-dependent pressure fluctuations. Rearrangement of the inviscid equations of motion, integrated across the jet's thickness led him to derive an ordinary differential equation describing the response of the jet's convergence length to applied pressure fluctuations. Finnicum et al. [14] investigated the static deflection of a liquid sheet under the influence of a constant pressure difference across the sheet. Their experiments showed good agreement with the simplified, global equations of motion for a two-dimensional inviscid sheet with surface tension. Furthermore, Weinstein et al. [15], and Clarke et al. [16] investigated the dynamic response of two-dimensional, inviscid liquid sheets subject to disturbances in ambient pressure. Based upon the assumption of potential flow, and by using perturbation methods, they derived linearised equations governing small deflections of a liquid sheet around a steady-state base flow. The derived approximate equation was validated by experiments.

Schmid and Henningson [17] investigated the stability of a liquid curtain, falling under the influence of gravity, and influenced by a compressible air cushion enclosed on one side of the curtain. They derived inviscid equations of motion, which were linearised on the assumption of small oscillations, compared to the length of the curtain. The linear system describes horizontal velocity and displacement of the curtain from the vertical axis. This system shows an instability feature, which was found to be in good agreement with experiments. The corresponding wave packet travels down the curtain and causes a strong pressure signal in the enclosed air cushion. Mehring and Sirignano [18] analysed linear and nonlinear dilational and sinuous capillary waves on thin, planar liquid sheets in the absence of gravity. They derived a time-dependent 1D system of equations in the assumption that the sheet is thin compared with the wavelength of the disturbance. In the linear system the equations governing the dilational and sinuous deflection are decoupled. The nonlinear equations are analysed separately for the case of dilational and sinuous waves. Good agreement is found with a 2D nonlinear system. They compared linear and nonlinear solutions to a harmonic forcing at the orifice, and found that nonlinear solutions do not change some of the character of sheet distortion identified by the linear analysis. However, in the nonlinear case higher harmonics, and in some cases sheet breakup were observed.

The present discussion makes clear that the above mentioned works are not able to fully describe the case under present investigation. The present study is concerned with the derivation of a good model describing large time-dependent deflections of a liquid sheet. These deflections originate from the acceleration of the sheet. Inertia forces will thus be important, and gravity must be included. Moreover, the present analysis will consider a viscous liquid, as the Reynolds number is found to be small in practice.

1.2. Article outline

The present article derives 2D equations of motion governing the time-dependent deflection of a liquid sheet when subjected to inertia forces. In Sections 2 and 3 the problem is mathematically posed. A curvilinear co-ordinate system is chosen, based on the *instantaneous* position of the sheet's centre line. Thereafter, the equations of motion are derived within the chosen reference frame, and boundary conditions at the free surfaces are derived. Section 4 makes the derived equations dimensionless. Based on the assumption of slender sheets, an order of magnitude analysis is performed, and the number of terms is reduced. Section 5 discusses the integration of the reduced equations of motion across the sheet. In order to calculate the pressure integrals, an expression for the pressure within the sheet is extracted from the boundary conditions at the interface. Integration of the equations of motion finally leads to a workable set of differential equations, that describe streamwise velocity, normal velocity of the centre line, and thickness in function of time. Section 6 adds a few comments on the derived set of equations, and compares the present set with equations found in literature. Section 7 finally investigates the effect of viscosity on the transient response of the sheet.

2. Initial considerations

Consider a liquid sheet, falling under the influence of gravity. The sheet is unsupported, meaning that it has two liquid–air interfaces. For the present study an interface between a viscous liquid with constant surface tension σ, and an inviscid gas is considered. The gas is only able to exert a pressure normal to the interface. Consider also the sheet to be infinitely wide (or wide enough such that the lateral ends of the sheet do not affect the dynamics in the middle). Thus, a two-dimensional analysis suffices to describe the motion of a sheet cross-section.

2.1. Co-ordinate system

In order to deal mathematically with the sheet's deflection, consider a curvilinear, orthogonal co-ordinate system (s, n) as depicted in Fig. 2. Here, the s-axis is orientated in streamwise direction, and assumes the instantaneous position of the sheet's centre line. The n-axis is normal to s. Only axis s is curved, and the angle that the s-axis makes with the vertical is denoted θ, as depicted in Fig. 2. The s-axis' curvature is represented by $\kappa = \partial\theta/\partial s$. As a time-dependent deflection of the sheet is considered, both θ and κ are function of time.

Fig. 2 also depicts an (x, y) Cartesian co-ordinate system, fixed to the coating die, and having its origin on the sheet's centre line, at the die outlet. The origin of the (s, n) frame coincides at all times with the origin of (x, y). The (x, y) frame is not inertial, as it undergoes acceleration of the die, denoted $\vec{a}_D$. In steady-state, $\theta \equiv 0$, and the (s, n) frame coincides with (x, y), with $\vec{s} = \vec{x}$ and $\vec{n} = -\vec{y}$. On the other hand, when axis s is curved, the length of an arc in between (s, n) and $(s + \delta s, n)$ depends upon the local curvature $\kappa(s, t)$ of axis s, and on the normal co-ordinate n. This arc length can be written as $(1 + n\kappa)\delta s$, and throughout this paper we use $h = 1 + n\kappa$, such that the length of an infinitesimal arc is denoted $h\delta s$.

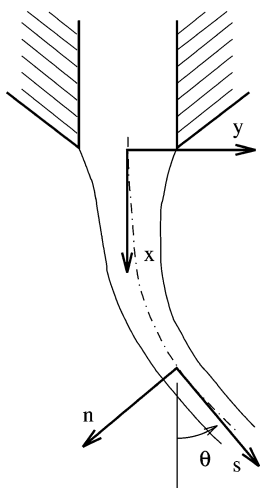

Fig. 2. Cross-section of a bent liquid sheet, and definition of a curvilinear co-ordinate system (s, n).

Equations of motion are derived in the moving (s, n) frame of reference, following an Eulerian approach (control volume approach). The velocity components in the (s, n) frame are represented by (u, v) along s and n respectively. (u, v) only describe flow within the sheet, and do not describe the velocity of deflection. The deflection is described by the motion of the s-axis, which is constructed to assume the instantaneous position of the sheet's centre line. The velocity of the centre line, *normal* to s, is represented by $f = f(s, t)$. As the centre line coincides at all times with the s-axis, f also represents the velocity of axis s. Note that f is independent of n. The centre line velocity f is seen by an observer moving with the (x, y) frame, but is *not* seen by an observer moving along with (s, n).

3. Equations of motion

Motivated by the discussion in Section 1.1, equations of motion will now be derived that describe the time-dependent behaviour of slender liquid sheets subjected to inertia forces. On the one hand the deflection of the sheet is assumed to be large, and in the authors' opinion a curvilinear reference frame is best suited in this case to describe motion. The derivation of the N–S equations in a steady curvilinear co-ordinate system has been repeatedly reported elsewhere.[1] On the other hand, in light of the discussion in Section 2.1, the curvilinear reference frame will be *unsteady* (i.e. κ is function of time). Such a reference frame has already been used by Buckmaster et al. [11] to derive equations for an inertialess flow. In this section, the full N–S equations are derived for inertia-gravity driven flow in a viscous liquid sheet.

3.1. Conservation of mass

The mass conservation equation is derived assuming a fixed fluid element as depicted in Fig. 3. With the aid of this figure, and following the reasoning of Lamb,[2] the mass conservation equation can easily be derived by stating that the net resultant mass flux through an infinitesimal element must equal the change of mass within the infinitesimal element:

$$-\rho\left\{\frac{\partial u}{\partial s}+\frac{\partial}{\partial n}(hv)\right\}\delta s\delta n=\frac{\partial}{\partial t}(\rho h\delta s\delta n).$$

Assuming a liquid of constant density, the mass conservation equation may thus be written as:

$$\frac{\partial h}{\partial t}+\frac{\partial u}{\partial s}+\frac{\partial}{\partial n}(hv)=0. \tag{6}$$

The first term $\partial h/\partial t$ in (6) results from the time-dependence of the (s, n) frame, and is therefore new w.r.t. previous expressions for mass conservation.

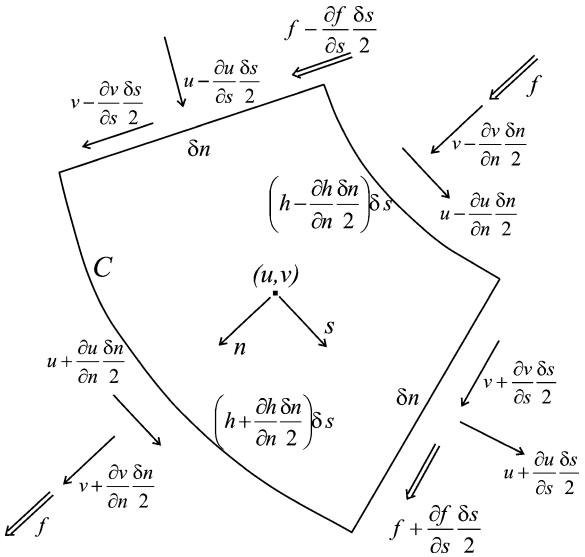

Fig. 3. Components of the velocity in an infinitesimal element centred round a point (s, n). The f-velocity component is not seen by an observer travelling along with the (s, n) frame.

[1] The authors used Goldstein [19], page 119.

[2] Lamb [20], Art. 7.

3.2. Momentum equations

Conservation of momentum states that the change in momentum of a fixed control volume $h\delta s\delta n$ is only due to forces acting on that control volume:[3]

$$\frac{\partial}{\partial t}\iint_A \rho(\vec{v}+\vec{f})\,\mathrm{d}A + \oint_C (\vec{v}+\vec{f})\big(\rho(\vec{v}+\vec{f})\,\mathrm{d}\vec{\ell}\big) = \sum \delta F. \tag{7}$$

The first term on the left-hand side of (7) is a surface integral over the surface of the control volume of Fig. 3. The second term is an integral taken along the contour of that fluid element.

The surface integral has components

$$\rho\frac{\partial}{\partial t}(hu)\delta s\,\delta n, \qquad \rho\frac{\partial}{\partial t}(hv+hf)\delta s\delta n \tag{8}$$

along s and n respectively, while the integral along the contour of an infinitesimal control area results in:

$$\begin{aligned} &\text{along } s\text{:} \quad \rho\left\{2u\frac{\partial u}{\partial s} + 2\kappa u(v+f) + hu\frac{\partial v}{\partial n} + h(v+f)\frac{\partial u}{\partial n}\right\}\delta s\delta n,\\ &\text{along } n\text{:} \quad \rho\left\{(v+f)\left(2h\frac{\partial v}{\partial n} + \frac{\partial u}{\partial s}\right) + u\left(\frac{\partial v}{\partial s} + \frac{\partial f}{\partial s}\right) - \kappa u^2 + \kappa(v+f)^2\right\}\delta s\delta n. \end{aligned} \tag{9}$$

An expression for the contribution of the forces acting on an infinitesimal element will now be derived. Gravity acts as a volume force on the element by its amount $\rho\vec{g}h\delta s\delta n$. Let the die be accelerated by $\vec{a}_D$, then the sheet experiences an inertial force $-\rho\vec{a}_D h\delta s\delta n$. For the moment no assumptions are made concerning the orientation of the sheet. Therefore, the components of $\vec{g}$ along axes x and y are denoted g_x and g_y respectively. For the inertial force $\vec{a}_D$, the components are a_{Dx} and a_{Dy}.

As the fluid is considered to be viscous, with constant dynamic viscosity μ, the internal stresses exert tractions on the boundaries of the infinitesimal element, as depicted in Fig. 4. Summing the tractions results in:

$$\begin{aligned} &\text{along } s\text{:} \quad \left\{\frac{\partial p_{ss}}{\partial s} + \frac{\partial}{\partial n}(hp_{ns}) + p_{ns}\frac{\partial h}{\partial n}\right\}\delta s\delta n,\\ &\text{along } n\text{:} \quad \left\{\frac{\partial p_{ns}}{\partial s} + \frac{\partial}{\partial n}(hp_{nn}) - p_{ss}\frac{\partial h}{\partial n}\right\}\delta s\delta n. \end{aligned} \tag{10}$$

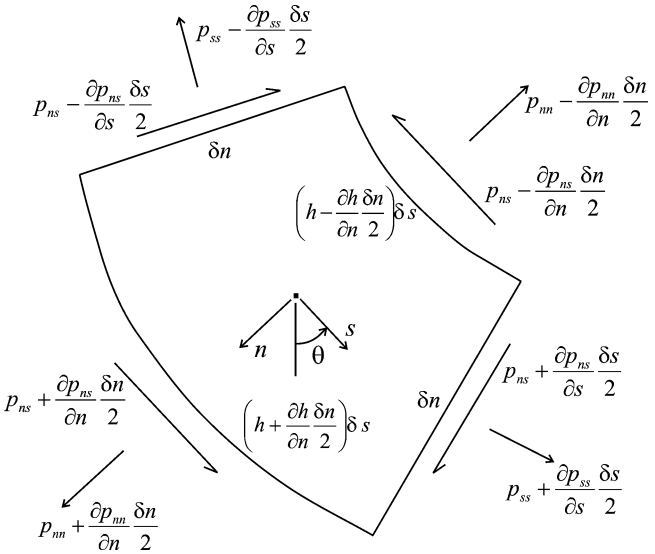

Fig. 4. Stresses exerted at the boundaries of an infinitesimal element.

[3] The authors used Streeter [21], Eq. (2.28).

The contribution of the tractions can be expressed in terms of the velocity components by means of the constitutive equations for the stresses (see Goldstein [19]):

$$\begin{aligned} p_{ss} &= -p + 2\mu\left\{\frac{1}{h}\frac{\partial u}{\partial s} + \frac{1}{h}\frac{\partial h}{\partial n}v\right\},\\ p_{nn} &= -p + 2\mu\frac{\partial v}{\partial n},\\ p_{ns} &= \mu\left\{\frac{1}{h}\frac{\partial v}{\partial s} + h\frac{\partial}{\partial n}\left(\frac{u}{h}\right)\right\}. \end{aligned} \tag{11}$$

The reader should note here that f does not enter (11), as the constitutive equations for the stresses are described within the (s, n) frame.

All terms of Eq. (7) have been derived. Thus, we substitute (8)–(10) with (11), and the expressions for the volume forces in the momentum equation (7). With the aid of (6), the momentum equations in differential form are found to be:

$$\begin{aligned} (s)\quad & \rho\left\{h\frac{\partial u}{\partial t} + u\frac{\partial u}{\partial s} + h(v+f)\frac{\partial u}{\partial n} + \kappa u(v+2f)\right\} = \rho h\left\{(g_x - a_{Dx})\cos\theta + (g_y - a_{Dy})\sin\theta\right\} - \frac{\partial p}{\partial s}\\ &\quad + \mu\left\{\frac{1}{h}\frac{\partial^2 u}{\partial s^2} + h\frac{\partial^2 u}{\partial n^2} - \frac{n}{h^2}\frac{\partial \kappa}{\partial s}\frac{\partial u}{\partial s} + \kappa\frac{\partial u}{\partial n} - \frac{\kappa^2}{h}u + \frac{1}{h^2}\frac{\partial \kappa}{\partial s}v + 2\frac{\kappa}{h}\frac{\partial v}{\partial s} + \frac{n^2}{h^2}\frac{\partial \kappa}{\partial t}\frac{\partial \kappa}{\partial s} - \frac{n}{h}\frac{\partial}{\partial s}\left(\frac{\partial \kappa}{\partial t}\right)\right\},\\ (n)\quad & \rho\left\{h\left(\frac{\partial v}{\partial t} + \frac{\partial f}{\partial t}\right) + u\left(\frac{\partial v}{\partial s} + \frac{\partial f}{\partial s}\right) + h(v+f)\frac{\partial v}{\partial n} - \kappa u^2 + \kappa f^2 + \kappa f v\right\}\\ &\quad = \rho h\left\{(g_x - a_{Dx})\sin\theta - (g_y - a_{Dy})\cos\theta\right\} - h\frac{\partial p}{\partial n}\\ &\quad + \mu\left\{\frac{1}{h}\frac{\partial^2 v}{\partial s^2} + h\frac{\partial^2 v}{\partial n^2} - \frac{n}{h^2}\frac{\partial \kappa}{\partial s}\frac{\partial v}{\partial s} + \kappa\frac{\partial v}{\partial n} - \frac{\kappa^2}{h}v - \frac{1}{h^2}\frac{\partial \kappa}{\partial s}u - 2\frac{\kappa}{h}\frac{\partial u}{\partial s} + \frac{n}{h}\kappa\frac{\partial \kappa}{\partial t} - \frac{\partial}{\partial n}\left(n\frac{\partial \kappa}{\partial t}\right)\right\}. \end{aligned} \tag{12}$$

Comparing (12) with the momentum equations given by Goldstein [19] (Eq. (7) page 119) for time-dependent flow along a fixed, curved wall shows that:

$$\rho\left\{hf\frac{\partial u}{\partial n} + 2\kappa u f\right\} \quad \text{and} \quad \rho\left\{h\frac{\partial f}{\partial t} + u\frac{\partial f}{\partial s} + hf\frac{\partial v}{\partial n} + \kappa(f^2 + fv)\right\}$$

represent additional momentum terms in an unsteady curvilinear frame, in s and n direction respectively. The term $2\kappa u f$ may be seen as the Coriolis acceleration of a particle moving along a curved path with velocity u and at the same time moving radially with velocity f. The first three terms for n correspond to the three rightmost terms of $(12, n)$, but with v replaced by f.

Comparison of the expressions for the viscous tractions with Goldstein [19] (Eq. (7) page 119) shows the following additional terms in (12):

$$\frac{n^2}{h^2}\frac{\partial \kappa}{\partial t}\frac{\partial \kappa}{\partial s} - \frac{n}{h}\frac{\partial}{\partial s}\left(\frac{\partial \kappa}{\partial t}\right) \quad \text{and} \quad \frac{n}{h}\kappa\frac{\partial \kappa}{\partial t} - \frac{\partial}{\partial n}\left(n\frac{\partial \kappa}{\partial t}\right)$$

for s and n respectively. These are related to the time-dependence of κ.

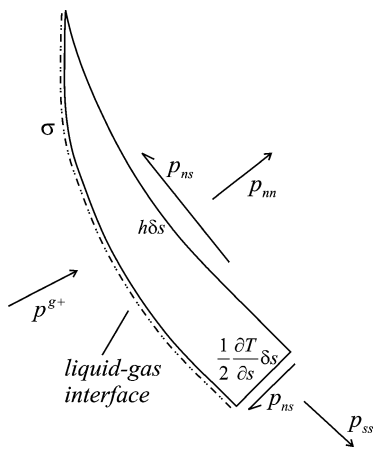

Fig. 5. Triangular boundary element at the positive interface.

3.3. Boundary conditions

At both liquid–air interfaces kinematic and dynamic boundary conditions must be applied. The kinematic boundary condition originates from the fact that the interface (in 2D) is a streamline. This consideration is expressed by the following relationship:

$$hv = \pm\frac{1}{2}\left(h\frac{\partial T}{\partial t} + u\frac{\partial T}{\partial s}\right) \quad \text{at } n = \pm\frac{T}{2}. \tag{13}$$

Here, T denotes the local sheet thickness. The dynamic boundary conditions are derived by writing out the momentum equations for a triangular boundary element as depicted in Fig. 5. They are derived in appendix, and result in the following expressions:

$$\begin{aligned}
(s^+)\quad & -\mu\left(\frac{\partial v}{\partial s} + h^+\frac{\partial u}{\partial n} - \kappa u\right) + \mu\frac{\partial T}{\partial s}\left(\frac{1}{h^+}\frac{\partial u}{\partial s} + \frac{\kappa}{h^+}v\right) + \frac{1}{2}\frac{\partial T}{\partial s}(p^{g+} - p^+ + \sigma\kappa_{if}^+) = 0,\\
(n^+)\quad & h^+p^+ - 2\mu h^+\frac{\partial v}{\partial n} + \frac{\mu}{2}\frac{\partial T}{\partial s}\left(\frac{1}{h^+}\frac{\partial v}{\partial s} + \frac{\partial u}{\partial n} - \frac{\kappa}{h^+}u\right) - h^+(p^{g+} + \sigma\kappa_{if}^+) = 0,\\
(s^-)\quad & \mu\left(\frac{\partial v}{\partial s} + h^-\frac{\partial u}{\partial n} - \kappa u\right) + \mu\frac{\partial T}{\partial s}\left(\frac{1}{h^-}\frac{\partial u}{\partial s} + \frac{\kappa}{h^-}v\right) + \frac{1}{2}\frac{\partial T}{\partial s}(p^{g-} - p^- - \sigma\kappa_{if}^-) = 0,\\
(n^-)\quad & -h^-p^- + 2\mu h^-\frac{\partial v}{\partial n} + \frac{\mu}{2}\frac{\partial T}{\partial s}\left(\frac{1}{h^-}\frac{\partial v}{\partial s} + \frac{\partial u}{\partial n} - \frac{\kappa}{h^-}u\right) + h^-(p^{g-} - \sigma\kappa_{if}^-) = 0,
\end{aligned} \tag{14}$$

where the $+$ sign is used to denote quantities at the interface for positive $n = T/2$, while the $-$ sign denotes quantities at the interface for negative $n = -T/2$. Note that κ_{if}^+ and κ_{if}^- represent the curvatures of the interfaces, which normally do not coincide with the s-axis' curvature κ.

The set of equations describing viscous flow in a liquid sheet is complete, consisting of Eqs. (6) and (12), describing viscous fluid flow, together with the boundary conditions (13) and (14). The next step will consist in making the terms nondimensional.

4. Nondimensional (normalised) form

The derived equations will now be expressed in a nondimensional fashion in order to assess the order of magnitude of the various terms in the equations. Therefore, we choose appropriate length and velocity scales.

An appropriate length scale for the present analysis is found by considering that the sheet deflections under investigation are on the order of the sheet length. The characteristic wavelength of these deflections is therefore proportional to the length of the sheet. Thus, let us choose the sheet length L to be the characteristic length scale for the streamwise direction.[4] Let us define a corresponding velocity scale $u_s = \sqrt{gL}$. The initial sheet thickness, T_0, is chosen as the length scale for the normal direction. Then $\varepsilon = T_0L^{-1}$ represents a slenderness ratio. The velocity scale for the normal velocity is $v_s = \sqrt{\varepsilon g T_0}$, such that $v_s = \varepsilon u_s$. In the present analysis we assume the sheet to be slender such that $\varepsilon \ll 1$. Furthermore, time is scaled by $\tau = Lu_s^{-1} = \sqrt{Lg^{-1}}$, and pressure by $\pi = \rho u_s^2 = \rho g L$.

Now all quantities may be expressed in nondimensional form, thus (overscore bar denotes dimensionless quantity):

$$\bar{s} = \frac{s}{L}, \quad \bar{n} = \frac{n}{T_0}, \quad \bar{t} = \frac{t}{\tau}, \quad \bar{u} = \frac{u}{u_s}, \quad \bar{v} = \frac{v}{v_s}, \quad \overline{T} = \frac{T}{T_0}, \quad \bar{p} = \frac{p}{\pi}, \quad \bar{\kappa} = L\kappa.$$

With these definitions $h = 1 + \varepsilon\bar{n}\bar{\kappa}$. As f will generally be much larger than v, let us assume:

$$\bar{f} = \frac{f}{u_s}.$$

Consider also a Reynolds number:

$$Re = \frac{\rho u_s T_0}{\mu} = \varepsilon\frac{\rho\sqrt{gL}L}{\mu} = \varepsilon R$$

such that the *modified* Reynolds number $R = \mathrm{O}(1)$. Likewise, consider a Weber number:

$$We = \frac{\rho u_s^2 T_0}{\sigma} = \varepsilon\frac{\rho g L^2}{\sigma} = \varepsilon W.$$

[4] The chosen length and velocity scales correspond to a long-wave analysis of the governing equations. See e.g. also Ramos [9].

Use will be made of the *modified* Weber number W in what follows, but a note should be made at this point concerning the order of magnitude of W. It is tempting to consider $W = \mathrm{O}(1)$, but this is mostly not the case as the ratio ρ/σ is very large, say $\mathrm{O}(\varepsilon^{-1})$. We will further address this issue in Section 6.

The nondimensional quantities are substituted into the equations of motion. All terms $\mathrm{O}(\varepsilon)$ or higher in Eqs. (6) and (12) are neglected, as their influence on the behaviour of the differential equations is negligible, compared to the terms that are retained. By so doing, and dropping the overscore bar, as all quantities are dimensionless, the following nondimensional equations are derived.

Mass conservation

$$\frac{\partial h}{\partial t} + \frac{\partial u}{\partial s} + \frac{\partial}{\partial n}(hv) = 0. \tag{15}$$

Momentum balance

$$\begin{aligned}
(s)\quad & h\frac{\partial u}{\partial t} + u\frac{\partial u}{\partial s} + hv\frac{\partial u}{\partial n} + \frac{h}{\varepsilon}f\frac{\partial u}{\partial n} + 2\kappa u f \\
&\quad = h\left\{\frac{g_x - a_{Dx}}{g}\cos\theta + \frac{g_y - a_{Dy}}{g}\sin\theta\right\} - \frac{\partial p}{\partial s} + \frac{1}{R}\left\{\frac{1}{h}\frac{\partial^2 u}{\partial s^2} + \frac{h}{\varepsilon^2}\frac{\partial^2 u}{\partial n^2} + \frac{\kappa}{\varepsilon}\frac{\partial u}{\partial n} - \frac{\kappa^2}{h}u\right\} + \mathrm{O}(\varepsilon), \\
(n)\quad & h\frac{\partial f}{\partial t} + u\frac{\partial f}{\partial s} + hf\frac{\partial v}{\partial n} - \kappa(u^2 - f^2) = h\left\{\frac{g_x - a_{Dx}}{g}\sin\theta - \frac{g_y - a_{Dy}}{g}\cos\theta\right\} - \frac{h}{\varepsilon}\frac{\partial p}{\partial n} \\
&\quad + \frac{1}{R}\left\{\frac{h}{\varepsilon}\frac{\partial^2 v}{\partial n^2} + \kappa\frac{\partial v}{\partial n} - \frac{1}{h^2}\frac{\partial \kappa}{\partial s}u - 2\frac{\kappa}{h}\frac{\partial u}{\partial s} - \frac{\partial}{\partial n}\left(n\frac{\partial \kappa}{\partial t}\right)\right\} + \mathrm{O}(\varepsilon).
\end{aligned} \tag{16}$$

Kinematic boundary condition

$$hv = \pm\frac{1}{2}\left(h\frac{\partial T}{\partial t} + u\frac{\partial T}{\partial s}\right) \quad \text{at } n = \pm\frac{T}{2}. \tag{17}$$

Dynamic boundary conditions, $\mathrm{O}(\varepsilon^2)$ accurate

$$\begin{aligned}
(s^+)\quad & -\frac{1}{R}\left\{\varepsilon\frac{\partial v}{\partial s} + \frac{h^+}{\varepsilon}\frac{\partial u}{\partial n} - \kappa u - \frac{\varepsilon}{h^+}\frac{\partial T}{\partial s}\frac{\partial u}{\partial s}\right\} + \frac{1}{2}\varepsilon\frac{\partial T}{\partial s}\left\{p^{g+} - p^+ + \frac{\kappa_{if}^+}{W}\right\} = 0, \\
(n^+)\quad & -h^+\left\{p^{g+} - p^+ + \frac{\kappa_{if}^+}{W}\right\} - \frac{2}{R}h^+\frac{\partial v}{\partial n} + \frac{1}{2R}\frac{\partial T}{\partial s}\left\{\frac{\partial u}{\partial n} - \frac{\varepsilon}{h^+}\kappa u\right\} = 0, \\
(s^-)\quad & \frac{1}{R}\left\{\varepsilon\frac{\partial v}{\partial s} + \frac{h^-}{\varepsilon}\frac{\partial u}{\partial n} - \kappa u + \frac{\varepsilon}{h^-}\frac{\partial T}{\partial s}\frac{\partial u}{\partial s}\right\} + \frac{1}{2}\varepsilon\frac{\partial T}{\partial s}\left\{p^{g-} - p^- - \frac{\kappa_{if}^-}{W}\right\} = 0, \\
(n^+)\quad & h^-\left\{p^{g-} - p^- - \frac{\kappa_{if}^-}{W}\right\} + \frac{2}{R}h^-\frac{\partial v}{\partial n} + \frac{1}{2R}\frac{\partial T}{\partial s}\left\{\frac{\partial u}{\partial n} - \frac{\varepsilon}{h^-}\kappa u\right\} = 0.
\end{aligned} \tag{18}$$

The dynamic boundary conditions will be used to derive an expression for the pressure. As the pressure term in the n-balance equation (16) is $\mathrm{O}(\varepsilon^{-1})$, terms in (18) are retained to $\mathrm{O}(\varepsilon)$.

5. Integration of the equations of motion

In order to get a workable set of equations describing the dynamic behaviour of a liquid sheet, the set of Eqs. (15) and (16) is integrated across the sheet. Calculation of the integrals is only possible when assumptions are made concerning the velocity profiles, and the pressure. An expression for the pressure is derived from the boundary conditions (18).

Motivated by the results of Söderberg and Alfredsson [6], which have been discussed in Section 1.1, we assume a uniform streamwise velocity profile

$$u = A(s,t) \quad \text{and} \quad \partial u/\partial n = 0 \tag{19}$$

which was also found by Ramos [9] as the leading order term of u. This assumption may also be deduced from looking at the momentum equations (16), where the terms containing $\partial u/\partial n$ appear to be $\mathrm{O}(\varepsilon^{-1})$. Such a large impact does not make sense in slender sheets, at least at a sufficient distance from the orifice. Thus, we postulate that $\partial u/\partial n$ should be at most $\mathrm{O}(\varepsilon)$ such that the terms in (16) containing these derivatives result to be O(1) or smaller. The same holds for $\partial^2 u/\partial n^2$ which is assumed to be $\mathrm{O}(\varepsilon^2)$ or smaller. Let us note here that (19) was found both by Ramos and Söderberg et al. for vertically falling liquid sheets,

for which in the present case $g_x = g$, and $g_y = 0$. When the sheet emanates from a direction that is significantly inclined w.r.t. the vertical, (19) may not hold, and an n-dependence of u should be considered, say $u = A(s,t) + \varepsilon C(s,t)n$. This assumption will be investigated in Section 6. Consider for the present case (19) to hold.

The present analysis assumes a profile for v, that varies linearly with n, and that is consistent with the kinematic boundary condition at both liquid-gas interfaces, thus

$$v = B(s,t)n. \tag{20}$$

Ramos [9] found (20) as the leading order term of v. A look at the n-balance of (16) makes clear that $\partial^2 v/\partial n^2$ should be at most $O(\varepsilon)$. The assumption of a nonzero $\partial^2 v/\partial n^2$ will be investigated in Section 6. Furthermore, let the interfacial curvature κ_{if} be written as $\kappa_{if}^{\pm} = \kappa + \tilde{\kappa}_{if}^{\pm}$. Expressions for the curvatures $\tilde{\kappa}_{if}^{\pm}$ at both interfaces are found when considering the interface of a planar sheet ($\kappa = 0$):

$$\tilde{\kappa}_{if}^{\pm} = \mp\frac{1}{2}\varepsilon\frac{\partial^2 T}{\partial s^2} + O(\varepsilon^2). \tag{21}$$

Integration of the mass conservation equation (15) across the sheet gives:

$$\varepsilon\frac{\partial \kappa}{\partial t}\int_{-T/2}^{T/2} n\,\mathrm{d}n + \int_{-T/2}^{T/2}\frac{\partial u}{\partial s}\,\mathrm{d}n + \int_{-T/2}^{T/2}\frac{\partial}{\partial n}(hv)\,\mathrm{d}n = 0.$$

The integral in the first term is zero. The time-dependence of κ thus disappears from the integral expression of the mass conservation equation. The remaining two integrals can be calculated with the aid of the kinematic boundary condition (17). The integral expression for mass conservation thus becomes:

$$\frac{\partial}{\partial s}(Tu) + \frac{\partial T}{\partial t} = 0. \tag{22}$$

Note that (22) has been derived independently of any assumption on the profile of the normal velocity v.

On the other hand, assuming a linear n-dependence of v as in (20), another interesting relationship may be deduced from the kinematic boundary condition (17). Subtracting the kinematic boundary condition at $n = -T/2$ from the one at $n = T/2$ gives:

$$h^+v^+ - h^-v^- = u\frac{\partial T}{\partial s} + \frac{\partial T}{\partial t}. \tag{23}$$

Expliciting the left-hand side of (23), using (20) results in:

$$h^+v^+ - h^-v^- = h^+\frac{T}{2}\frac{\partial v}{\partial n} + h^-\frac{T}{2}\frac{\partial v}{\partial n} = T\frac{\partial v}{\partial n}. \tag{24}$$

Comparing (24) with (23) leads to the following expression:

$$T\frac{\partial v}{\partial n} = u\frac{\partial T}{\partial s} + \frac{\partial T}{\partial t}, \tag{25}$$

and comparing (25) with the integral form of the equation for mass conservation (22) leads to:

$$\frac{\partial u}{\partial s} + \frac{\partial v}{\partial n} = 0. \tag{26}$$

The u and v velocity components are thus always interrelated, independent of the time-behaviour of the sheet. As will be shown in Section 6, the accuracy of (26) is $O(\varepsilon)$. (26) can also be derived directly from the mass conservation equation (15), when neglecting terms of $O(\varepsilon)$, and holds even for large deflections (i.e. $\kappa = O(1)$).

To integrate the momentum equations (16) across the sheet, expressions for the integrals of the pressure derivatives $\partial p/\partial s$ and $\partial p/\partial n$ are needed. These are derived from the dynamic boundary conditions in appendix. With the aid of (22) and (26), the momentum equations (16), integrated across the sheet, result in the following expressions:

$$\begin{aligned}
(s)\quad & \frac{\partial u}{\partial t} + u\frac{\partial u}{\partial s} + 2\kappa u f = \frac{g_x - a_{Dx}}{g}\cos\theta + \frac{g_y - a_{Dy}}{g}\sin\theta \\
& \quad - \frac{1}{2}\frac{\partial}{\partial s}\{p^{g+} + p^{g-}\} + \frac{1}{R}\left\{4\frac{\partial^2 u}{\partial s^2} + \frac{4}{T}\frac{\partial T}{\partial s}\frac{\partial u}{\partial s} - \kappa^2 u\right\} + O(\varepsilon), \\
(n)\quad & \frac{\partial f}{\partial t} + u\frac{\partial f}{\partial s} - f\frac{\partial u}{\partial s} - \kappa(u^2 - f^2) = \frac{g_x - a_{Dx}}{g}\sin\theta - \frac{g_y - a_{Dy}}{g}\cos\theta - \frac{1}{\varepsilon T}\{p^{g+} - p^{g-}\} - \frac{1}{\varepsilon T}\frac{2\kappa}{W} \\
& \quad - \frac{1}{R}\left\{\frac{1}{T}\frac{\partial T}{\partial s}\kappa u + 3\kappa\frac{\partial u}{\partial s} + u\frac{\partial \kappa}{\partial s} + \frac{\partial \kappa}{\partial t}\right\} + O(\varepsilon).
\end{aligned} \tag{27}$$

The two integral momentum equations (27), together with the integral form of the mass conservation equation (22), constitute a set of equations of motion in the unknowns u, f, and T. The shape of the s-axis, characterised by θ and κ can be derived by integration of the velocity f over time.

6. Discussion of the validity of the equations

This section first discusses accuracy issues related to the derived set of equations (27), especially in light of the assumed velocity profiles (19) and (20). A necessary comparison of the derived set with previous literature follows.

The equations of motion (22) and (27) have been derived considering a streamwise velocity u independent of the normal co-ordinate n, as shown by (19). In Section 5 it was noted from (16), that $\partial u/\partial n$ is at most $\mathrm{O}(\varepsilon)$. The assumption $\partial u/\partial n = 0$ actually implies that for a bent sheet, fluid particles at the concave side of the sheet will reach a certain location downstream faster than particles at the convex side. This is readily discerned by looking at the expression for the element of length $h = 1 + n\kappa$. Physically speaking, this means that some additional viscous force will be present. This viscous force will now be identified.

Suppose the hypothesis from the theory of elasticity, stating that planar cross-sections remain planar after bending, is considered valid also for sheet flow. Then, an expression for the dependence of u on n may be deduced in the sense:

$$u = A(s,t) + \varepsilon C(s,t)n. \tag{28}$$

Here A is the average streamwise velocity, as the integral of the second term on the right across the sheet is zero. An expression for C may be deduced when forcing planar cross sections to remain planar after flowing over an infinitesimal distance downstream, such that $h\delta s = u\delta t$. Equalling terms in the same power of ε results in:

$$C = \kappa A. \tag{29}$$

Likewise, from the discussion in Section 5 it is clear that $\partial^2 v/\partial n^2 = \mathrm{O}(\varepsilon)$ or smaller. Assume thus:

$$v = B(s,t)n + \varepsilon D(s,t)n^2. \tag{30}$$

Redoing the derivation of the equations and boundary conditions with the new expressions (28) and (30), for u and v respectively, results finally in slightly altered momentum equations with respect to (27). The newly found s-momentum balance has, compared with (27), on its left-hand side an additional inertia term Cf, and on its right-hand side an additional viscous term $\kappa C R^{-1}$. Using (29) this means that the additional viscous term cancels the last viscous term in the s-balance of (27). The newly derived n-momentum balance has additional viscous terms $-2DR^{-1}$ and $C(\partial T/\partial s)(TR)^{-1}$ with respect to (27). Using (29) this last viscous term cancels the first viscous term in the n-balance of (27). Clearly (29) reduces viscous dissipation in a bent liquid sheet. This analysis is $\mathrm{O}(\varepsilon)$ accurate.

When (28) and (30) are used to derive (26), it can be shown that $B = -\partial A/\partial s$ is $\mathrm{O}(\varepsilon)$ accurate. In (27) viscous terms appear of $\mathrm{O}(1)$. As already noted by Clarke [5], this shows that viscosity still plays a relevant role in the flow behaviour of slender liquid sheets, even on the assumption of a uniform streamwise velocity (19). We will further assess the influence of viscosity by means of numerical computations in Section 7.

A closer look at the n-balance equation of (27) reveals a pressure and surface tension term of $\mathrm{O}(\varepsilon^{-1})$. We deduce thus that an $\mathrm{O}(\varepsilon)$ pressure difference $p^{g+} - p^{g-}$ will cause an $\mathrm{O}(1)$ deflection of the sheet. In Section 4 it was already noted that $W \approx \mathrm{O}(\varepsilon^{-1})$, so the surface tension term is globally $\mathrm{O}(1)$ too.

For stationary, vertically falling liquid sheets ($g_x = g$ and $g_y = 0$), without any applied acceleration $\vec{a}_D = 0$, and with $p^{g+} = p^{g-}$, the sheet's centre line is straight. Under such circumstances $\theta(s) = \kappa(s) = 0$. The s-momentum balance thus becomes:

$$u\frac{\partial u}{\partial s} = 1 + \frac{1}{R}\left\{4\frac{\partial^2 u}{\partial s^2} - 4\frac{1}{u}\left(\frac{\partial u}{\partial s}\right)^2\right\}, \tag{31}$$

which coincides with equation (2) of Taylor, when applying the normalisation procedure given by (1). Let us recall that (2) was also derived by Clarke [5] and Ramos [9] as the leading order equation governing the streamwise velocity in slender, viscous liquid sheets. Comparing (31) with Aidun's equation (5) shows an additional surface tension and pressure term in (5). Our present analysis also includes surface tension effects, but these do not appear in (31) because it was shown that $\tilde{\kappa}_{if} = \mathrm{O}(\varepsilon)$. The pressure term in (5) appears because Aidun expressed dynamic boundary conditions with only the surface tension balancing the stresses at the interface, while not considering the pressure (Eq. (7) in [8]).

Finnicum et al. [14] derived an equation governing the deflection of an inviscid sheet based on an overall momentum balance in a curvilinear reference frame. Eqs. (4) of Finnicum et al. are also predicted by the presently derived Eqs. (27). In fact, in

the time-*independent* case, for an inviscid liquid and under a constant pressure difference, (27) rewritten in *dimensional* form becomes:

$$(s)\quad \frac{\partial}{\partial s}(Tu^2) = gT\cos\theta,$$
$$(n)\quad \kappa(Tu^2 - 2\sigma) = (p^{g+} - p^{g-}) - \rho g T \sin\theta \tag{32}$$

which is identical to the set of equations (4) of Finnicum et al.

Weinstein et al. [15] derived time-dependent equations governing the shape of a 2D liquid sheet for very small deflections of the sheet's centre line. Inviscid, potential flow is assumed, and the equations are linearised around an undisturbed base flow. In essence, Weinstein et al. derived two equations, one governing the deflection of the sheet's centre line, which they call the sinuous equation, and a second one governing thickness variations, which is called the varicose equation, for the case that a pressure disturbance is applied. The varicose equation (Eq. (25b) in Weinstein et al.) is nothing else than the integral form of the continuity equation (22) derived in the present paper. The sinuous equation deserves a closer look. The dimensional counterpart of the sinuous equation (25a) of Weinstein et al. is:

$$\frac{\partial^2 Y}{\partial t^2} + 2u\frac{\partial^2 Y}{\partial x \partial t} + \left\{u^2 - \frac{2\sigma}{\rho T}\right\}\frac{\partial^2 Y}{\partial x^2} = -g\frac{\partial Y}{\partial x} + \frac{p^{g+} - p^{g-}}{\rho T} \tag{33}$$

in which Y represents the y-co-ordinate of the centre line, and all other quantities are represented by the definitions adopted in the present paper. (33) is valid for Y very small. We will now try to express the n-balance of (27) in the same form of (33). Assume inviscid flow, and very small deflections such that $f = \mathrm{O}(\varepsilon)$. Redoing the derivation under these assumptions does not introduce any additional terms than present in (27). Thus, the following *dimensional* equation governs the deflection in the inviscid case, for small f, $g_x = g$, $g_y = 0$ and $\vec{a}_D = 0$:

$$\frac{\partial f}{\partial t} + u\frac{\partial f}{\partial s} - f\frac{\partial u}{\partial s} - \left\{u^2 - \frac{2\sigma}{\rho T}\right\}\kappa = g\sin\theta - \frac{p^{g+} - p^{g-}}{\rho T}. \tag{34}$$

For small f, $\vec{s} \approx \vec{x}$, and by considering the kinematic condition at a boundary interface:[5]

$$-f = \frac{\partial Y}{\partial t} + u\frac{\partial Y}{\partial x} \tag{35}$$

an expression for the time derivative of f may be deduced. The minus sign appears due to the orientation of the (s, n)-frame. For deriving the spatial derivative of f, the diffusion term in (35) may not be considered: $\partial f/\partial s = -\partial^2 Y/\partial x \partial t$. Furthermore $\kappa \approx \partial^2 Y/\partial x^2$ and $\sin\theta = \partial Y/\partial x$. Comparing now the two equations, we note that in (33) a term $-f\,\partial u/\partial s$ is missing with respect to (34). This term originates from the term $\rho h(v + f)\partial v/\partial n$ in Eq. (12) and does not disappear after integration as it is an even function of n. It may however be argued that when f is very small this term might be neglected.

Eq. (33) is identical to the one derived by Schmid and Henningson [17] for an inviscid falling liquid curtain (Eq. (2.6)). Those authors used a derivation similar to Weinstein et al. The nonlinear equations derived by Mehring and Sirignano [18] governing capillary waves on horizontal, inviscid liquid sheets may also be deduced following the derivation described in the present paper. In this case a different scaling method should be applied, as gravity is not included in the analysis of Mehring and Sirignano. In this context a slenderness ratio still can be used, but refers to the ratio of the sheet thickness to a characteristic wavelength of the appearing capillary waves. The terms appearing on the right-hand side of Eqs. (2.21) and (2.22) of Mehring and Sirignano are surface tension terms due to the curvature of the interface and of the centre line. In the present analysis they were – except for the capillary term in the n-balance – neglected as their order of magnitude resulted to be too small.

A solution to the presently derived Eqs. (22) and (27) in the case of an applied acceleration $\vec{a}_D$ may be found by numerical methods as the following section describes.

7. Influence of viscosity

This section investigates to which extent the transient response of a liquid sheet is affected by viscosity. The analysis is based on numerical computations of the derived set of Eqs. (22) and (27) by a finite difference method. A predictor–corrector algorithm was used to solve the finite difference equations for the three unknowns T, u, and f. This is an explicit finite-difference method to solve the equations through a time-marching scheme. It is $\mathrm{O}(\Delta s^2)$ accurate in both time and space. Calculations were performed with Matlab™ with a time step of 5.0×10^{-5} s. The sheet consisted of 50 nodes. The computations were

[5] See e.g. Mehring and Sirignano [18], or Schmid and Henningson [17].

performed assuming the following values: length of the sheet $L = 0.125$ m, $\rho = 1100\ \mathrm{kg\,m^{-3}}$, $\sigma = 37 \times 10^{-3}\ \mathrm{N\,m^{-1}}$, initial sheet thickness $T_0 = 0.4$ mm, and flow rate per unit sheet width $Q = 100\ \mathrm{mm^2\,s^{-1}}$. Using these values, the slenderness ratio $\varepsilon = 3.2 \times 10^{-3}$, and the streamwise velocity scale $u_s = 1.1\ \mathrm{m\,s^{-1}}$. Pressure differences across the sheet are not considered for this analysis: $p^{g+} = p^{g-}$.

In the stationary case of a vertically falling sheet ($g_x = g$, and $g_y = 0$), for which no $\vec{a}_D$ is applied and $f(s,t) \equiv 0$ at all times, the stationary streamwise velocity and sheet thickness can be found by large-time computation of the finite difference equations. Stationary values of u and T have been computed for viscosities $\mu = 0.01$ Pa s, $\mu = 1$ Pa s, and $\mu = 10$ Pa s. The corresponding values of the modified Reynolds number are: $R = 15\,220$, $R = 152.2$, and $R = 15.2$ respectively. Fig. 6 plots the results. The curves for $\mu = 0.01$ Pa s coincide with the free fall velocity under gravity and are therefore labelled as *inviscid*. An increasing viscosity will slow down the streamwise velocity and cause a thicker sheet. The difference in streamwise velocity at the lower end of the sheet, compared with the inviscid case, amounts to 5% for $\mu = 1$ Pa s and 24% for $\mu = 10$ Pa s.

The shown differences in the stationary u and T for viscous liquids, compared to the inviscid case will undoubtedly affect the transient response of the sheet to an applied acceleration $\vec{a}_D$. We will illustrate the influence with a computed example. Consider

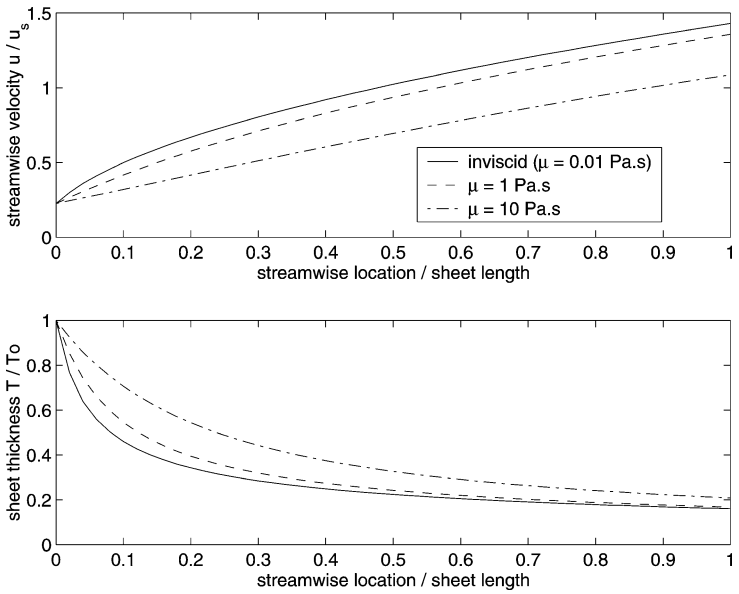

Fig. 6. Computed stationary streamwise velocity and sheet thickness (nondimensional values).

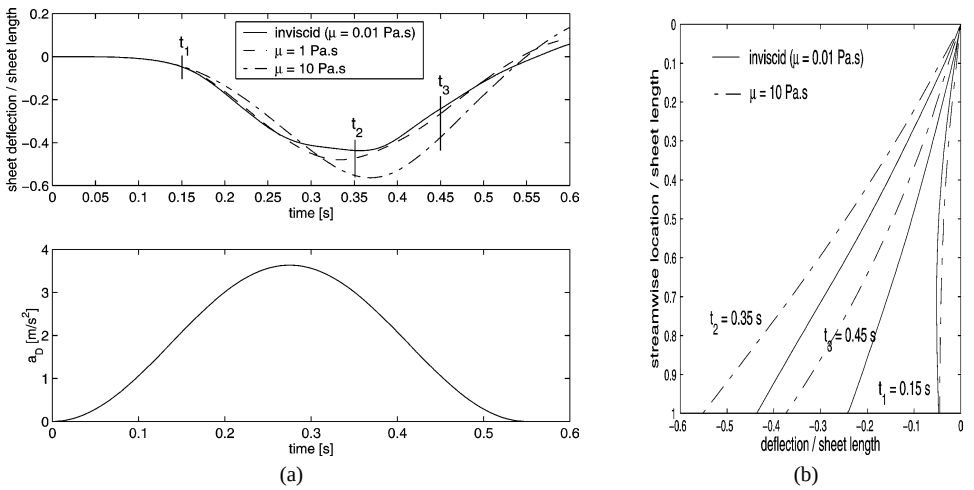

Fig. 7. Computed transient responses of a sheet for different liquid viscosities. (a) Deflection of sheet's lower end and applied a_D. (b) Sheet profile during deflection.

an acceleration: $a_{Dx} = 0$, $a_{Dy} = a_D(t)$ shown in the lower graph of Fig. 7(a). The computed transient response of the sheet to this applied acceleration trajectory is given in Fig. 7 for different values of viscosity. Fig. 7(b) shows the lateral sheet profiles at three instances of time. The upper graph of Fig. 7(a) plots the normalised horizontal (y) displacement of the sheet's lower end in function of time. The graphs show that a higher viscosity causes (i) a slower response and (ii) an increased deflection of the sheet. The use of higher performing acceleration trajectories (i.e. with higher peak accelerations) will accentuate the differences. Let us also note that the present computations assume a sheet in a vacuum. Surrounding air will significantly affect the response during sheet motion. For a detailed discussion on this aspect the interested reader is referred to part II, which discusses performed experiments and compares with additional computational results.

8. Conclusion

The aim of this part I paper was to derive equations of motion capable of describing the time-dependent deflection of a sheet of liquid when subjected to inertia forces. Liquid viscosity was considered in the derivation. The equations of motion have been derived in a curvilinear co-ordinate system which is time-dependent, its shape being governed by θ and κ. The derived equations of motion are integral expressions over the sheet's thickness, and constitute a set in the unknowns u, f, and T.

The integral continuity equation governs the unsteady sheet thickness. The integral s-momentum balance governs the unsteady streamwise velocity, orientated along the sheet's centre line, and the integral n-momentum balance provides a time-dependent equation governing the normal velocity of the sheet's centre line. The derived equations are $O(\varepsilon)$ accurate.

The derived equations predict equations governing streamwise velocity, large steady-state deflections and small time-dependent deflections that were derived in previous literature works. Finally, an analysis was performed to investigate the influence of viscosity on the sheet's behaviour, based on finite difference computations of the derived equations. The influence of viscosity on the streamwise velocity was found to be significant. The response of a viscous sheet to an applied acceleration trajectory is larger and slower, compared to the inviscid case.

Part II will present experimental data of the response of a liquid sheet to various a_D. Experiments are then compared to numerical computations, based on the set of integral equations derived in the present paper.

Acknowledgements

Part of this research was supported by a research grant from the Flemish Institute for the Promotion of Innovation through Science and Technology (I.W.T.).

The authors would like to express their gratitude to the anonymous referees for their useful comments and suggestions, which have helped improve the paper.

Appendix A. Derivation of the dynamic boundary conditions at a free surface

In order to derive the dynamic boundary conditions at a free liquid–air interface we follow the thoughts of Buckmaster [10] and write out the momentum equations for a triangular boundary fluid element, as depicted in Fig. 5. Therefore, we explicit Eq. (7), and note that the surface integral on the left-hand side of (7) is $O(\delta s^2)$, and we therefore neglect it. The same holds for the volume forces. The integral along the contour is zero, because the fluxes through the borders cancel out totally. Therefore, the resulting equations will not contain any inertia terms. This is in contrast with Buckmaster's expressions (2.4) [10]. The problem here is that Buckmaster apparently did not consider a flux through the interface. The present authors note here that due to a fixed control volume approach, there has to be a flux through the interface if the interface is to change. This fact may also be seen when considering that the u, v, and f velocity components at the interface are not orientated along the interface. The resulting dynamic boundary conditions at the positive interface thus result in the following expressions:

$$\begin{aligned} (s^+) \quad & -h^+ p_{ns} + \frac{1}{2}\frac{\partial T}{\partial s} p_{ss} + \frac{1}{2}\frac{\partial T}{\partial s}(p^{g+} + \sigma\kappa_{if}^+) = 0, \\ (n^+) \quad & -h^+ p_{nn} + \frac{1}{2}\frac{\partial T}{\partial s} p_{ns} - h^+(p^{g+} + \sigma\kappa_{if}^+) = 0. \end{aligned} \tag{A.1}$$

The the $+$ sign is used to denote quantities at the interface for positive $n = T/2$, and κ_{if}^+ represents the curvature of this interface, which normally does not coincide with the s-axis' curvature κ. Analysis of (A.1) shows that the present derivation equals the statement that the stress tensor at the edges is balanced by ambient pressure and surface tension, as is also assumed in Ramos [9].

The derivation for the negative interface proceeds analogously, and results in:

$$\begin{aligned}(s^-)\quad & h^- p_{ns} + \frac{1}{2}\frac{\partial T}{\partial s} p_{ss} + \frac{1}{2}\frac{\partial T}{\partial s}(p^{g-} - \sigma\kappa_{if}^-) = 0,\\ (n^-)\quad & h^- p_{nn} + \frac{1}{2}\frac{\partial T}{\partial s} p_{ns} + h^-(p^{g-} - \sigma\kappa_{if}^-) = 0.\end{aligned} \tag{A.2}$$

Expressions (A.1) and (A.2) can be written in terms of the velocity components with the aid of (11) and result in (14).

Appendix B. Calculation of the integrals of the pressure derivatives

First, an expression for the pressure p in the sheet is derived from the n-balances of the dynamic boundary conditions (18). Considering (19), these may be rewritten to:

$$\begin{aligned}p^+ &= p^{g+} + \frac{\kappa}{W} - \frac{1}{2}\frac{\varepsilon}{W}\frac{\partial^2 T}{\partial s^2} + \frac{1}{R}\left\{2\frac{\partial v}{\partial n} + \frac{1}{2}\frac{\varepsilon}{h^{+2}}\frac{\partial T}{\partial s}\kappa u\right\} + \mathrm{O}(\varepsilon^2),\\ p^- &= p^{g-} - \frac{\kappa}{W} - \frac{1}{2}\frac{\varepsilon}{W}\frac{\partial^2 T}{\partial s^2} + \frac{1}{R}\left\{2\frac{\partial v}{\partial n} - \frac{1}{2}\frac{\varepsilon}{h^{-2}}\frac{\partial T}{\partial s}\kappa u\right\} + \mathrm{O}(\varepsilon^2).\end{aligned} \tag{B.1}$$

When the terms of $\mathrm{O}(\varepsilon^2)$ or higher in (B.1) are neglected, an expression for the pressure p within the sheet can be derived:

$$p = \frac{1}{T}\left\{\left(n + \frac{T}{2}\right)p^{g+} - \left(n - \frac{T}{2}\right)p^{g-}\right\} + \frac{2n}{T}\frac{\kappa}{W} - \frac{1}{2}\frac{\varepsilon}{W}\frac{\partial^2 T}{\partial s^2} + \frac{1}{R}\left\{2\frac{\partial v}{\partial n} + \frac{\varepsilon}{h^{-2}}\frac{n}{T}\frac{\partial T}{\partial s}\kappa u\right\} + \mathrm{O}(\varepsilon^2). \tag{B.2}$$

For calculating the integrals, we first need two other relationships, that can also be deduced from the dynamic boundary conditions (18). Summing the s-balances of (18) gives:

$$\frac{1}{2}\frac{\partial T}{\partial s}\left\{(p^{g+} + p^{g-}) - (p^+ + p^-)\right\} - \frac{1}{R}\left\{T\frac{\partial B}{\partial s} - 2\frac{\partial T}{\partial s}\frac{\partial u}{\partial s}\right\} = \mathrm{O}(\varepsilon), \tag{B.3}$$

while summing the n-balances of (18) results in the following equation:

$$(p^+ - p^-) - (p^{g+} - p^{g-}) + \varepsilon\kappa\frac{T}{2}\left\{(p^+ + p^-) - (p^{g+} + p^{g-})\right\} - \frac{2\kappa}{W} - \frac{\varepsilon}{R}\left\{2\kappa T B + \frac{\partial T}{\partial s}\kappa u\right\} = \mathrm{O}(\varepsilon^2). \tag{B.4}$$

The integral of the s-derivative of the pressure can be written as:

$$\int_{-T/2}^{T/2}\frac{\partial p}{\partial s}\mathrm{d}n = \frac{\partial}{\partial s}\int_{-T/2}^{T/2} p\,\mathrm{d}n - \frac{1}{2}\frac{\partial T}{\partial s}(p^+ + p^-). \tag{B.5}$$

Inserting (B.3) into (B.5), and using (B.2) leads to:

$$\int_{-T/2}^{T/2}\frac{\partial p}{\partial s}\mathrm{d}n = \frac{T}{2}\frac{\partial}{\partial s}(p^{g+} + p^{g-}) + \frac{1}{R}\left\{2\frac{\partial}{\partial s}(TB) + T\frac{\partial B}{\partial s} - 2\frac{\partial T}{\partial s}\frac{\partial u}{\partial s}\right\} + \mathrm{O}(\varepsilon). \tag{B.6}$$

The integral of the n-derivative of the pressure may be written out as follows.

$$\int_{-T/2}^{T/2} h\frac{\partial p}{\partial n}\mathrm{d}n = \int_{-T/2}^{T/2}\frac{\partial p}{\partial n}\mathrm{d}n + \varepsilon\kappa\int_{-T/2}^{T/2} n\frac{\partial p}{\partial n}\mathrm{d}n = (p^+ - p^-) + \varepsilon\kappa\left[\int_{-T/2}^{T/2}\frac{\partial}{\partial n}[np]\mathrm{d}n - \int_{-T/2}^{T/2} p\,\mathrm{d}n\right]. \tag{B.7}$$

With the aid of (B.4), and (B.2) the integral (B.7) becomes:

$$\int_{-T/2}^{T/2} h\frac{\partial p}{\partial n}\mathrm{d}n = (p^{g+} - p^{g-}) + \frac{2\kappa}{W} + \frac{\varepsilon}{R}\frac{\partial T}{\partial s}\kappa u + \mathrm{O}(\varepsilon^2). \tag{B.8}$$

The accuracy of (B.8) has to be $\mathrm{O}(\varepsilon^2)$, as the term containing $\partial p/\partial n$ in (16) is $\mathrm{O}(\varepsilon^{-1})$, and the set (27) is accurate to $\mathrm{O}(\varepsilon)$.

References

[1] S.F. Kistler, P.M. Schweizer, Liquid Film Coating – Scientific Principles and their Technological Implications, Chapman & Hall, 1997.
[2] M. Gilio, J.-P. Kruth, P. Vanherck, High-speed curtain recoating for stereolithography, in: D. Bourell (Ed.), Proc. 12th Solid Freeform Fabrication Symposium, 2001, pp. 46–54.
[3] J.-P. Kruth, M.C. Leu, T. Nakagawa, Progress in additive manufacturing and rapid prototyping, Ann. CIRP 48 (2) (1998) 525–540.
[4] D.R. Brown, A study of the behaviour of a thin sheet of moving liquid, J. Fluid Mech. 10 (1961) 297–305.
[5] N.S. Clarke, Two-dimensional flow under gravity in a jet of viscous liquid, J. Fluid Mech. 31 (3) (1968) 481–500.
[6] L.D. Söderberg, P.H. Alfredsson, Experimental and theoretical stability investigations of plane liquid sheets, Eur. J. Mech. B Fluids 17 (5) (1998) 689–737.
[7] K. Adachi, Laminar jets of a plane liquid sheet falling vertically in the atmosphere, J. Non-Newtonian Fluid Mech. 24 (1987) 11–30.
[8] C.K. Aidun, Mechanics of a free-surface liquid film flow, Trans. ASME J. Appl. Mech. 54 (1987) 951–954.
[9] J.I. Ramos, Planar liquid sheets at low Reynolds numbers, Int. J. Numer. Methods Fluids 22 (1996) 961–978.
[10] J. Buckmaster, The buckling of thin viscous jets, J. Fluid Mech. 61 (3) (1973) 449–463.
[11] J.D. Buckmaster, A. Nachman, L. Ting, The buckling and stretching of a viscida, J. Fluid Mech. 69 (1) (1975) 1–20.
[12] S.J. Weinstein, K.J. Ruschak, Coating flows, Annu. Rev. Fluid Mech. 36 (2004) 29–53.
[13] J.I. Ramos, Dynamic response of liquid curtains to time-dependent pressure fluctuations, Appl. Math. Modelling 15 (2) (1991) 126–135.
[14] D.S. Finnicum, S.J. Weinstein, K.J. Ruschak, The effect of applied pressure on the shape of a two-dimensional liquid curtain falling under the influence of gravity, J. Fluid Mech. 255 (1993) 647–665.
[15] S.J. Weinstein, A. Clarke, A.G. Moon, E.A. Simister, Time-dependent equations governing the shape of a two-dimensional liquid curtain, part 1: theory, Phys. Fluids 9 (12) (1997) 3625–3636.
[16] A. Clarke, S.J. Weinstein, A.G. Moon, E.A. Simister, Time-dependent equations governing the shape of a two-dimensional liquid curtain, part 2: experiment, Phys. Fluids 9 (12) (1997) 3637–3644.
[17] P.J. Schmid, D.S. Henningson, On the stability of a falling liquid curtain, J. Fluid Mech. 463 (2002) 163–171.
[18] C. Mehring, W.A. Sirignano, Nonlinear capillary wave distortion and disintegration of thin planar liquid sheets, J. Fluid Mech. 388 (1999) 69–113.
[19] S. Goldstein (Ed.), Modern Developments in Fluid Dynamics, vol. 1, first ed., Dover, 1965.
[20] H. Lamb, Hydrodynamics, sixth ed., Cambridge University Press, 1932.
[21] V.L. Streeter (Ed.), Handbook of Fluid dynamics, first ed., McGraw-Hill, 1961.